ResearchGate

See discussions, stats, and author profiles for this publication at: https://www.researchgate.net/publication/231651739

Physicochemical Characteristics and Catalytic Activity of Alumina-Supported Nanosized Ceria–Terbia Solid Solutions

ARTICLE *in* THE JOURNAL OF PHYSICAL CHEMISTRY C · JANUARY 2009

Impact Factor: 4.77 · DOI: 10.1021/jp809837g

CITATIONS
31

READS
20

3 AUTHORS:

Benjaram M Reddy
CSIR-Indian Institute of Chemical Technolo…
280 PUBLICATIONS **5,707** CITATIONS
SEE PROFILE

Pranjal Saikia
Gauhati University
30 PUBLICATIONS **441** CITATIONS
SEE PROFILE

Pankaj Bharali
Tezpur University
38 PUBLICATIONS **621** CITATIONS
SEE PROFILE

Available from: Pranjal Saikia
Retrieved on: 02 February 2016

Physicochemical Characteristics and Catalytic Activity of Alumina-Supported Nanosized Ceria−Terbia Solid Solutions

Benjaram M. Reddy,* Pranjal Saikia, and Pankaj Bharali

Inorganic and Physical Chemistry Division, Indian Institute of Chemical Technology, Hyderabad 500 607, India

Sang-Eon Park

Laboratory of Nano-Green Catalysis, Department of Chemistry, Inha University, Incheon 402-751, Republic of Korea

Martin Muhler and Wolfgang Grünert

Lehrstuhl für Technische Chemie, Ruhr-Universität Bochum, D-44780 Bochum, Germany

Received: November 7, 2008; Revised Manuscript Received: December 15, 2008

Alumina-supported ceria−terbia solid solution (CeO_2-TbO_2/Al_2O_3 = 80:20:100 mol % based on oxides) has been synthesized and analyzed by means of different complementary techniques, namely, X-ray diffraction (XRD), Raman spectroscopy (RS), transmission electron microscopy (TEM), X-ray photoelectron spectroscopy (XPS), ion scattering spectroscopy (ISS), temperature programmed reduction/oxidation (TPR−TPO), UV−vis diffuse reflectance spectroscopy (UV−vis DRS), BET surface area, and thermogravimetry (TG−DTA). The primary purpose of this investigation was to understand the structural and catalytic properties of ceria−terbia solid solutions dispersed over alumina support and their thermal stability. XRD studies revealed formation of ceria−terbia solid solutions without phase segregation up to the investigated temperature range of 1073 K. No specific inactive compounds were formed between the alumina support and cerium or terbium oxides. As revealed by TEM, the sizes of the Ce−Tb oxide are in the nanometer range (average size ∼3.7−11.5 nm). The investigated combination catalyst exhibited a high specific surface area and better thermal stability. The RS measurements suggested the presence of oxygen vacancies due to defective structure formation. Both cerium and terbium are present in 3+ and 4+ oxidation states as per the XPS information. ISS studies revealed some surface enrichment of cerium in the extreme periphery of the catalyst surface. The solid solution particles are well distributed over the support surface. As a result of solid solution formation and high dispersion over the support, the reduction temperature of Ce−Tb mixed oxide is observed to be lower than its unsupported form inferring better redox properties. A significantly high OSC and CO oxidation activity is also exhibited by the alumina-supported Ce−Tb oxide system.

Introduction

Being a unique functional rare earth material, ceria (CeO_2) has been widely applied in different fields such as catalysis, sensors, electronics, optics, and so on.[1−13] Owing to strong absorption in the ultraviolet (UV) region, it has also been used as a UV blocking and shielding material.[14,15] In catalysis, the most significant use of ceria is in reducing the emissions of toxic pollutants from automobile exhaust. The ability of ceria to cycle between 3+ and 4+ oxidation states is the key factor for these applications. However, it is not easy to reduce bulk ceria at moderate temperatures and doping ceria with other oxides is one of the best options in order to get materials of increased reducibility and thereby superior catalytic activity. Interestingly, though it is a general perception that the dopant will increase the reducibility of ceria, the role of the second oxide may be much more subtle[9] because the enhanced activity may be due to the surface area stabilization or due to the increase in ionic conductivity of ceria making oxygen from the bulk more accessible for surface reactions.[9] By virtue of any one of these effects or both, fortunately, several ceria-based composite oxides are reported to comprise the remarkable ability to regulate oxygen storage and release properties and, therefore, these materials are now gaining interest for three-way-catalyst (TWCs, which control CO, NOx, and hydrocarbon emissions from automobiles) formulations.[16] Among them, the ceria−zirconia combination has attracted prime importance.[17−20] However, it is now well established that redox and ionic properties, and the thermal stability of ceria could be improved by incorporation of dopants other than Zr such as La, Hf, Gd, Pr, Y, and particularly Tb.[21−26] Some reports could be found in the literature on Ce−Tb mixed oxides.[26−31] Interestingly, ceria modification by doping with terbium has resulted in materials with enhanced catalytic properties for oxidation reactions due to better oxygen storage−release characteristics.[26,27,32−34]

Under operating conditions, TWCs have to withstand very high temperature and oscillating chemical environment. The major drawback of ceria-based TWCs is that they deactivate easily under these circumstances. Therefore, modern TWCs require new redox materials with an enhanced oxygen storage−release capacity (OSC) and wide temperature range sustainability.[16] Sintering or particle growth, leading to the

* Address correspondence to this author.

10.1021/jp809837g CCC: $40.75 © 2009 American Chemical Society
Published on Web 01/20/2009

deterioration of the OSC function, has been recognized as the major TWC deactivation pathway.[4] Therefore, a lot of attention has been focused in the literature on the stabilization of dispersed ceria or ceria comprised mixed oxides on high surface area materials such as alumina,[14,18,35] silica, titania, and others.[36−38] In the recent past, well-dispersed alumina supported ceria and ceria−zirconia mixed oxides are almost exclusively used in the commercial TWC preparation technology.[17−20,39] Motivated by these facts, the interest of using alumina as the support material for other ceria-based materials has experienced a rapid growth. Additionally, these systems could find use as efficient carriers for noble metal catalyts for other important industrial catalytic processes.[40] Very recently, we reported the efficiency of ceria−terbia solid solution in comparison to ceria toward enhancement of OSC and CO oxidation ability.[11] Investigation of ceria−terbia solid solutions supported on alumina is therefore a logical extension of our previous research on unsupported Ce−Tb mixed oxides.[11] It is known that reduced ceria reacts with alumina support to form the perovskite $CeAlO_3$ phase, leading to deactivation of the catalyst.[41−43] Of course, the formation of $CeAlO_3$ is responsible for the structural stabilization of alumina (helping in surface area stabilization) at very high temperatures under reductive conditions but the benefits of having CeO_2 in the catalyst formulation can be partially lost if ceria is replaced by other inactive or less active components.[44,45] Some attempts could be found in the literature where the alumina surface is modified with other substances.[16,46] Though this has been a useful step, we cannot deny the complexity of the resulting materials. Against this background, the present work has been undertaken. In this study, a highly dispersed Ce−Tb solid solution has been synthesized on a preformed alumina support and subjected to thermal treatments up to 1073 K, which correspond to the moderate thermal conditions of practical automotive exhaust gases.[47] The physicochemical characterization has been performed by using different techniques, namely, Brunauer−Emmett−Teller (BET) surface area, thermogravimetry (TG−DTA), X-ray diffraction (XRD), Raman spectroscopy (RS), transmission electron microscopy (TEM), X-ray photoelectron spectroscopy (XPS), ion scattering spectroscopy (ISS), UV−vis diffuse reflectance spectroscopy (UV−vis DRS), and temperature programmed reduction/oxidation (TPR−TPO). The catalytic performance was evaluated for oxygen storage/release capacity and CO oxidation activity.

Experimental Procedures

Catalyst Preparation. Alumina-supported ceria−terbia (CTA; Al_2O_3:CeO_2:TbO_2 = 100:80:20 mol % based on oxides) sample was prepared by a deposition coprecipitation method with use of dilute aqueous NH_3 solution. Powdered γ-Al_2O_3 (Harshaw) having a specific surface area of 127 $m^2\ g^{-1}$ was first dispersed in about 2000 mL of deionized water and stirred for 2 h. Second, ammonium cerium(IV) nitrate (Loba Chemie, GR grade) and terbium(III) nitrate (Aldrich, AR grade) were dissolved separately in deionized water and mixed together. Then under stirring condition, the two solutions were thoroughly mixed and the whole mixture was diluted to 4000 mL with deionized water. The stirring was continued for another 1 h. Aqueous NH_3 solution was added dropwise to the mixture until pH ∼8.5, under vigorous stirring. The obtained precipitate was filtered off, washed several times with deionized water, and oven-dried at 393 K for 12 h, then subsequently calcined at 773 K for 6 h in air atmosphere. Some portions of the finished catalyst were further calcined at 873, 973, and 1073 K, respectively, for 6 h. After cooling, the solid residues were ground with a ceramic mortar and pestle until fine powders were obtained.

Catalyst Characterization. The catalyst samples were analyzed by X-ray diffraction with use of a Rigaku Multiflex instrument equipped with nickel-filtered Cu Kα (0.15418 nm) radiation source and a scintillation counter detector. The intensity data were collected over a 2θ range of 2−80° with a 0.02° step size and a counting time of 1 s per point. The XRD phases present in the samples were identified with the help of Powder Diffraction File International Center for Diffraction Data (PDF-ICDD). The average crystallite size of the oxide phases was estimated with the help of the Scherrer equation and the lattice parameter was calculated by a standard cubic indexation method, using the intensity of the most prominent peak (111).[48]

The Raman spectra were recorded with a LabRam HR800UV Raman spectrometer (Horiba Jobin-Yvon) equipped with a confocal microscope and liquid-nitrogen cooled charge-coupled device (CCD) detector. The emission line at 325 nm from the He−Cd laser (Melles Griot Laser) was focused on the sample under the microscope, with the diameter of the analyzed spot being ∼1 μm. The time of acquisition was adjusted according to the intensity of Raman scattering. The wavenumber values reported from the spectra are accurate to within 1 cm^{-1}. To ascertain the homogeneity of the sample, spectra were recorded at various points and compared. All samples were found to be highly homogeneous.

The BET surface areas were determined by N_2 physisorption at liquid N_2 temperature on a Micromeritics Gemini 2360 instrument. Prior to analysis, the samples were oven-dried at 393 K for 12 h and flushed with Argon gas for 2 h. The thermogravimetric measurements were carried out on a Mettler Toledo TG−SDTA instrument. The catalyst sample was heated from ambient to 1273 K under nitrogen flow maintaining the heating rate at 10 deg min^{-1}.

The XPS measurements were made on a Shimadzu (ESCA 3400) spectrometer by using Mg Kα (1253.6 eV) radiation as the excitation source. Charging of the catalyst samples was corrected by setting the binding energy maximum of the adventitious carbon (C 1s) at 284.6 eV.[49] The analysis was done at room temperature and pressures were typically on the order of less than 10^{-8} Pa. The samples were outgassed in a vacuum oven overnight before XPS measurements. Quantitative analysis of atomic ratios was accomplished by determining the elemental peak areas, following the Shirley background subtraction.[49]

IS spectra were measured with a Leybold surface analysis system equipped with X-ray and ion sources and an EA 10/100 electron (ion) analyzer with multichannel detection (Specs). The samples were pretreated in flowing synthetic air (20% O_2/N_2) at 573 K for 30 min before they were introduced into the spectrometer vacuum without further contact with the ambient humid atmosphere (in situ treatment). The measurements were done with 3000 eV Ar^+ ions and recorded with the analyzer in pass-energy mode. The surface charge was removed with a flood gun. The source and the flood gun were allowed to stabilize with the sample withdrawn from the measurement position. Signal intensities were estimated assuming the background to be linear.

The UV−vis DRS measurements were performed over the wavelength range 200−700 nm, using a GBS-Cintra 10e UV−vis NIR spectrophotometer with integration sphere diffuse reflectance attachment. Samples were diluted in a KBr matrix by pelletization.

The TEM−HREM studies were made on a JEM-2010 (JEOL) instrument equipped with a slow-scan CCD camera and at an

accelerating voltage of 200 kV. Samples were sonically dispersed in ethanol and deposited on a carbon-coated copper grid before examination.

The TPR−TPO measurements of the 773 K calcined CTA sample were performed in a system equipped with a thermal conductivity detector. Before starting TPR runs, the sample was activated under flowing O_2 (9.35%)/Ar at 573 K for 30 min maintaining the heating rate of 10 deg min^{-1}. The sample was then cooled to 273 K. TPR was then performed by heating the sample at 5 deg min^{-1} up to 1073 K in a H_2 (4.2%)/Ar flow (84.1 mL min^{-1}). The sample was held at 1073 K for 1 h. The TPO experiment was performed following TPR after the sample was cooled in H_2 (4.2%)/Ar flow to 273 K. Then the sample was again heated to 1073 K at a rate of 10 deg min^{-1} under a flow of O_2 (5%)/Ar (100 mL min^{-1}). Thereafter, the reoxidized sample was allowed to cool in the O_2 (5%)/Ar (100 mL min^{-1}) environment to 273 K and the second reduction run (TPR-2) was carried out followed by the second oxidation run (TPO-2) under the same conditions as the first TPR−TPO runs.

OSC Measurements. A thermogravimetric method, essentially similar to that described previously elsewhere, was used to determine the OSC by the oxygen release characteristics of the sample in the temperature region 573−1073 K.[47,50] The change in the weight of the sample was monitored by thermogravimetry (TG) under cyclic heat treatments in flowing nitrogen or dry air. A commercial Netzsch TG−DTA analyzer (Luxx, STA, 409 PC, Germany) was employed for this purpose. The heat cycle consisted of heating the sample to 1073 K, cooling to 423 K, and again heating to 1073 K. All heating and cooling rates were maintained at 5 deg min^{-1}. The weight loss of the sample during the second heating cycle was used to measure the oxygen release properties.

CO Oxidation Activity. The CO oxidation activity of the synthesized catalysts was evaluated at normal atmospheric pressure and temperatures in the range of 300−773 K in a fixed bed microreactor at a heating ramp of 5 deg min^{-1}. About 100 mg of catalyst sample (250−355 μm sieve fraction) diluted with quartz particles of the same sieve fraction was placed in a quartz reactor for evaluation. Temperature was measured directly at the catalyst bed, using a thermocouple placed in the hollow part of the reactor. The following gases and gas mixtures were used (supplied by Air Liquide): argon (>99.999% purity), 9.98% CO in argon (CO purity, >99.997%; argon purity, >99.99%), and 10.2% O_2 in argon (oxygen purity, >99.995%). The total flow rates maintained by three mass flow controllers were in the range of 50−60 NmL min^{-1} (milliliters normalized to 273.15 K and 1 atm.). The CO and CO_2 gas concentrations were measured by using an Uras 14 infrared analyzer module, and the O_2 concentration was measured with a Magnos 16 analyzer (Hartmann & Braun). Prior to oxidation of CO, the catalysts were heated to 773 K in 10.2% O_2/Ar gas mixture, using a heating ramp of 10 deg min^{-1}, and kept at the final temperature for 1 h. The oxidized sample was then purged in argon and cooled to the desired starting temperature. The CO/O_2 reactant feed ratio was 1, and partial pressures of CO and O_2 were in the range of 10 mbar.

Results and Discussion

Thermal stability of the CTA sample was evaluated from TG−DTA analysis. The temperature suitable for calcination of the sample was also chosen on the basis of this analysis, at which the mass loss is stabilized. Two distinct features were mainly observed in the TG−DTA profile. One low-temperature feature (at around 353−373 K) observed was due to the loss of molecularly absorbed water from the surface. Another feature was noticed in the temperature range of 493−693 K, which could be attributed to the loss of impurities from the bulk. Above this temperature the weight loss was almost completely stabilized. On this basis, the primary calcination temperature for the catalyst sample was chosen to be 773 K. Up to 840 K, the total weight loss was calculated to be 9.66%, whereas from 840 to 1273 K, it was observed to be only 0.54%. Thus thermogravimetric analysis clearly revealed that the sample is thermally quite stable at high temperatures and could be used in high-temperature applications.

TABLE 1: BET Surface Area, Average Crystallite Size, and *a* Cell Parameter of Alumina-Supported Ce−Tb Mixed Oxide Calcined at Different Temperatures

sample/ calcination temp (K)	surface area (m^2 g^{-1})	crystallite size (nm)[a]	cell parameter "*a*" (Å)
CTA-773	148	3.73	5.38
CTA-873	128	4.59	5.38
CTA-973	114	5.78	5.39
CTA-1073	97	11.57	5.39

[a] From XRD analysis with the Scherrer equation

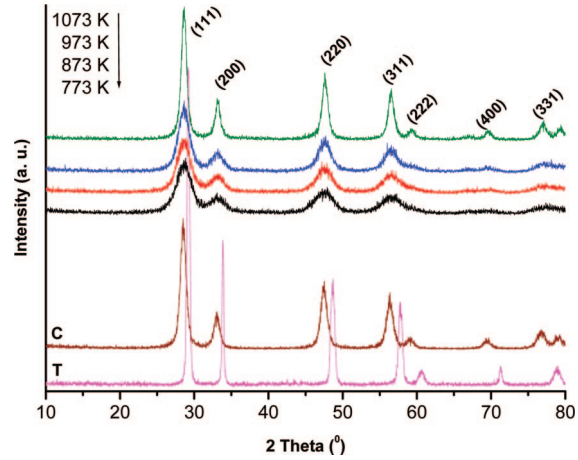

Figure 1. Powder XRD patterns of alumina supported ceria−terbia (CTA) samples calcined at different temperatures along with 773 K calcined CeO_2 (C) and terbium oxide (T).

The BET surface areas of the samples after thermal treatment at different temperatures (773−1073 K) are summarized in Table 1. The pure ceria and ceria−terbia (CT) samples prepared under identical conditions by adopting the same preparation technique exhibited surface areas of 41 and 85 m^2 g^{-1}, respectively, when calcined at 773 K.[11,51] These values were decreased to 8 and 37 m^2 g^{-1}, respectively, when the temperature was raised to 1073 K (i.e., 80.5% and 56.5% surface area decrease, respectively). In the present case, as given in the Table 1, the alumina-supported Ce−Tb oxide samples revealed reasonably high BET surface area: 148 m^2 g^{-1} for 773 K calcined sample, which gradually decreased to 97 m^2 g^{-1} after calcination at 1073 K, showing only 34.5% surface area loss. Thus the effect of alumina support is quite obvious.

X-ray diffraction data were collected for all CTA samples after calcination in the temperature range from 773 to 1073 K and the patterns are shown in Figure 1. For comparison purposes, XRD patterns of pure cerium oxide calcined at 773 K and terbium oxide are also included in the figure. The formation of solid solution between ceria and terbia is clearly noticed and no other species are detected. The diffraction peaks could be indexed to (111), (200), (220), (311), (222), (400),

and (331) crystal faces corresponding to a fluorite-type structure of ceria−terbia mixed oxide. The broadened lines indicate the presence of smaller particles of nanometer size. The average crystallite sizes of the Ce−Tb mixed oxides estimated with use of the Scherrer equation are presented in Table 1. For the 773 K calcined sample it was found to be ∼3.7 nm, which is gradually increased to ∼11.5 nm after heat treatment at 1073 K. The corresponding crystallite size values obtained for unsupported ceria−terbia mixed oxide were 5.5 and 12.1 nm, respectively.[11] The increased dispersion of the mixed oxide over the support with significant increase in the surface area might be the cause for this result. The increase in crystallite size values with increasing calcination temperature is supported by the gradual sharpening of the XRD peaks which could be rationalized as a result of sintering. Thus, the observation indicates an improvement in the crystallinity with corresponding increase in crystallite size and decrease in specific surface area after calcination at 873−1073 K (Table 1). The lattice parameters of the supported mixed oxide samples are slightly larger (5.38−5.39 Å) than that of the bulk mixed oxide of the same nominal chemical composition (5.36−5.37 Å).[11] This may indicate the presence of trivalent cations in the lattice of the resulting supported oxides, namely Ce^{3+} and Tb^{3+} or both, having cationic radii of 1.14 and 1.04 Å, respectively. As these cations are bigger than the tetravalent Ce^{4+} (cationic radius 0.97 Å), they can compensate for the contraction of the ceria lattice due to the presence of smaller Tb^{4+} (cationic radius 0.88 Å). However, the *a* cell parameter values for the mixed oxide samples (both supported and unsupported) are smaller than those for ceria (unit cell constant $a = 5.410$ Å). This observation opens up another possibility of incorporation of Al^{3+} cations with cationic radius of 0.51 Å into the ceria lattice other than Tb^{4+}. Literature reveals that in the case of ceria−alumina combination, within the temperature range of 673−973 K, the reduction of ceria to nonstoichiometric CeO_{2-x} is favored and subsequently diffusion of Al^{3+} into the partially reduced ceria lattice may lead to the $CeAlO_3$ formation.[52] There is another possibility that all Tb may not be fully incorporated in the process of mixed oxide formation with ceria and part of it may react with alumina counterpart to form $TbAlO_3$. However, in the present case, as stated earlier, no evidence is available regarding the presence of any species other than ceria−terbia solid solution within the investigated temperature range. This is an important observation in terms of the catalytic activity of the sample. However, we cannot rule out the possibility of the presence of terbia in the amorphous state being beyond the limit of XRD detection. In the case of 1073 K calcined sample, the cell parameter value is marginally high. This may be due to the presence of trivalent cations (Ce^{3+} and/or Tb^{3+}) in slightly higher amount in this sample. The XRD patterns simply reveal the single-phase patterns for the Ce−Tb oxides without phase segregation even after calcination at 1073 K. However, the peak widths of the nanosized materials are relatively large and therefore it is not easy to draw an exact conclusion if small amounts of segregated phases are present.

Vibrational spectroscopy is a powerful tool for characterizing the molecular structure of supported metal oxides. Raman spectroscopy has added advantages over IR spectroscopy when the supports used are specially γ-alumina and amorphous silica, because they absorb strongly below 1000 cm^{-1} and thus the IR bands of the metal oxide species are generally masked by those bands. But Raman bands of these oxide supports are very weak or Raman inactive in the same region.[53] Again, as the Raman spectrum of each molecular structure is unique, Raman spectroscopy can discriminate between different molecular structures of the supported metal oxides.[54] In the present study, Raman spectra are collected by using ultraviolet wavelength excitation (325 nm). In general, the spectra measured at two types of wavelengths (UV and visible) are more or less similar in terms of vibrational bands observed. However, depending on the nature and condition of the samples, Raman shift and intensity of the patterns may change. Raman spectral patterns of alumina-supported Ce−Tb oxides calcined at different temperatures are shown in Figure 2. The spectra of pure ceria (calcined at 773 and 1073 K) and terbium oxide are presented in the inset of the figure. The visible Raman spectrum of pure ceria (prepared by adopting the coprecipitation method and calcined at 773 K) reveals only one peak at 462 cm^{-1} due to the F_{2g} Raman-active mode characteristic of the fluorite structure of CeO_2.[51] However, a UV−Raman spectrum of the same sample shows that particular peak at ∼469 cm^{-1} (inset of Figure 2). Most probably, a small degree of hydration causes this band shift.[54] Additionally, a weak band at ∼260 cm^{-1} and a shoulder at ∼600 cm^{-1} are also observed, which can be attributed respectively to the Raman inactive (but IR active) transverse and longitudinal optical phonon modes at the Brillouin zone center.[55] The presence of these peaks is normally attributed to the perturbation of the fluorite structure. Interestingly, for all CTA samples, the peak at ∼600 cm^{-1} is relatively more pronounced, which reveals some structural changes in the cubic fluorite structure of ceria

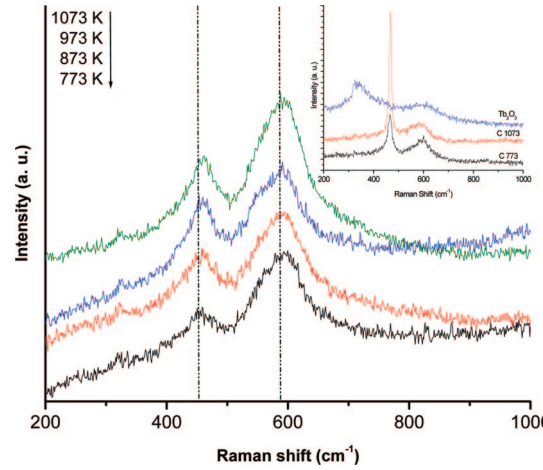

Figure 2. Raman spectra of alumina-supported ceria−terbia (CTA) samples calcined at different temperatures. [Inset: CeO_2 (C, 773 and 1073 K calcined) and terbium oxide (Tb_2O_3).]

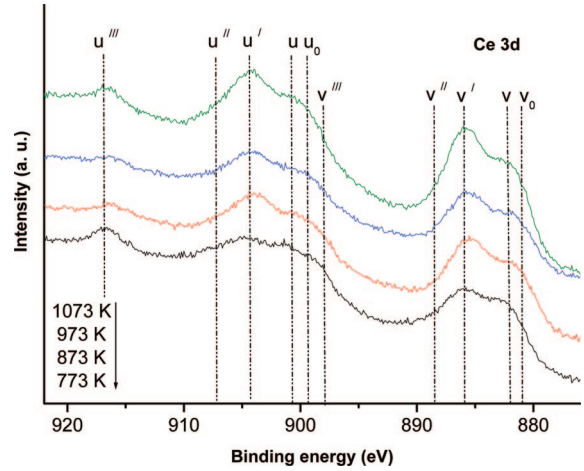

Figure 3. Ce 3d XPS patterns of alumina-supported ceria−terbia (CTA) samples calcined at different temperatures.

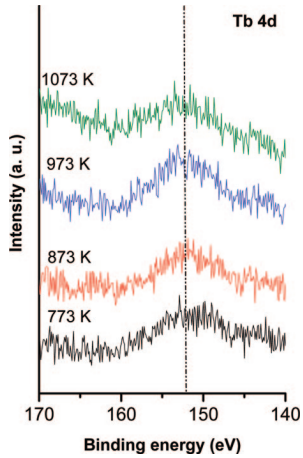

Figure 4. Tb 4d XPS patterns of alumina-supported ceria−terbia (CTA) samples calcined at different temperatures.

TABLE 2: XPS Core-Level Atomic Ratios of Alumina-Supported Ce−Tb Mixed Oxide Calcined at Different Temperatures

	atomic ratio	
sample/calcination temp (K)	Ce/Tb	Ce/Al
CTA-773	1.81	0.23
CTA-873	1.81	0.23
CTA-973	1.84	0.24
CTA-1073	1.83	0.22

after incorporation of terbium into its lattice. This band is also linked to the oxygen vacancies in the CeO_2 lattice.[56,57] The nature of the patterns may be due to the resonance enhancement of the Raman scattering cross section under UV excitation.[54] It is also known that depending on the system under study, there is a possibility for the resonance Raman scattering to be largely quenched due to a short lifetime for the electronically excited state.[54] Therefore, we may observe the low intensity of the F_{2g} band in the case of the mixed oxide samples. With increasing calcination temperature, a slight increase in the intensity of the peaks is noticed due to better crystallization of the mixed oxides at higher calcination temperatures.[52] No shift in band positions or emergence of new bands are noted for all the samples implying the homogeneous nature of the samples even after high thermal treatment. As can be observed from the inset of the figure, pure Tb_2O_3 reveals one main peak at ∼333 cm^{-1} and a shoulder at ∼600 cm^{-1}. The Raman spectra of the mixed oxide samples do not show the first peak. However, there is a possibility that the second peak at ∼600 cm^{-1} may be present and has overlapped with the peak, which has been ascertained due to the defective structure of ceria. This may be another reason for the pronounced nature of the peak in the ∼600 cm^{-1} region. However, from XRD analysis there is no clue about the presence of the crystalline terbia phase.

From the O 1s core electron level XPS profiles of CTA samples after thermal treatment at 773−1073 K, it is observed that all the patterns consist of very broad peaks centered at 531 eV assigned to the lattice oxygens associated with the oxides. The asymmetric nature of the peaks can be attributed to the different environments for oxides of Ce, Tb, and Al. The very flat nature of the peaks may mask any probable shoulder toward the high binding energy side, which is more likely to be present due to absorbed oxygen or to surface hydroxyl species and/or absorbed water present as contaminant at the surface.[40] As the temperature is increased, the peaks become sharpened due to the better crystallization of the samples. No pertinent difference in the binding energy maxima is noticed with temperature change, which indicates that the chemical state of the oxides remains unaltered.

Due to the hybridization of the O 2p valence band with the Ce 4f level, the Ce 3d core level XPS pattern of ceria is very complicated resulting in several final states for cerium and a number of overlapping peaks.[26,58] As can be seen from Figure 3, the Ce 3d spectrum consists of two sets of spin−orbit multiplets featuring $3d_{3/2}$ and $3d_{5/2}$ (represented as u and v respectively) contributions. The peaks at ∼882.1 eV (v) and 900.8 eV (u) are the main lines corresponding to the Ce^{4+} state whereas features at 888.5 (v″), 897.9 (v‴), 907.2 (u″), and 916.8 eV (u‴) are satellites related to this state. The main signals of Ce^{3+} (v_0, u_0) are generally noticed at around 881 and 898 eV, respectively. Here, it can be seen that the latter peak is overlapping with v‴. The satellites to these features (v′ and u′) occur at 885.9 and 904.2 eV, respectively. It can be observed that the shoulder above 881 eV is made up of a mixture of v and v_0 features and the usual good separation between v and v″ (characteristic of only Ce^{4+} state) is prevented by a significant intensity of v′ indicating the presence of Ce^{3+} in the sample. The presence of the Ce^{4+} state is supported by the considerable intensity of the u‴ peak. Thus, on the surface of the samples, the concentrations of both Ce^{4+} and Ce^{3+} are quite comparable. With an increase in the calcination temperature, the intensity of the peaks at ∼885 eV (v′) and ∼904 eV (u′) increased and that of the peak at ∼916 eV (u‴) decreased suggesting a higher amount of Ce^{3+} in the samples treated at higher temperatures.

The Tb 4d core level XPS spectra of the CTA samples calcined at different temperatures are presented in Figure 4. In the case of Tb it is difficult to have a unique agreement on the oxidation states of terbium. In fact, literature reports related to the Tb XPS (whether it may be Tb 3d or Tb 4d) are very limited. The Tb 3d core level analysis is more difficult with a conventional spectrometer due to the very low kinetic energies of the photoemitted electrons. It is, however, reported that in the Tb 4d XPS pattern, Tb^{3+} gives a signal below 150 eV whereas Tb^{4+} shows features above 150 eV.[59,60] As can be noticed from the figure, the spectra are very broad showing the maximum at ∼152 eV, with pronounced shoulders below 150 eV and a tailing toward 160 eV. This indicates that Tb may be present in both 3+ and 4+ oxidation states. With increasing calcination temperature, a small increase in the intensity of the peak maxima is observed (which is of course present above 150 eV) suggesting the presence of Tb^{4+} in relatively higher amounts than Tb^{3+}.

The Al 2p core level XPS patterns for the CTA samples consisted of peaks centered at 74.2 eV. Dufresne et al. reported the binding energy of Al^{3+} in alumina (amorphous or γ-alumina) at 74.8 eV.[61] In the literature, however, a large range of binding energies (73.7−74.8 eV) could be found for the Al 2p core level of alumina.[31,49] It is noticed that all the patterns look alike, with the intensity slightly enhancing with the temperature increase possibly due to better crystallization of the support. From these observations, it can be inferred that there is no formation of any mixed oxide compounds between alumina and ceria and/or terbia, which already has been substantiated by XRD analysis.

As presented in Table 2, the atomic ratios for Ce/Tb and Ce/Al did not change considerably when the temperature was increased from 773 to 1073 K. This indicates that there is no change of composition, or in other words, no further reaction occurred among the components within the temperature range of 773−1073 K.

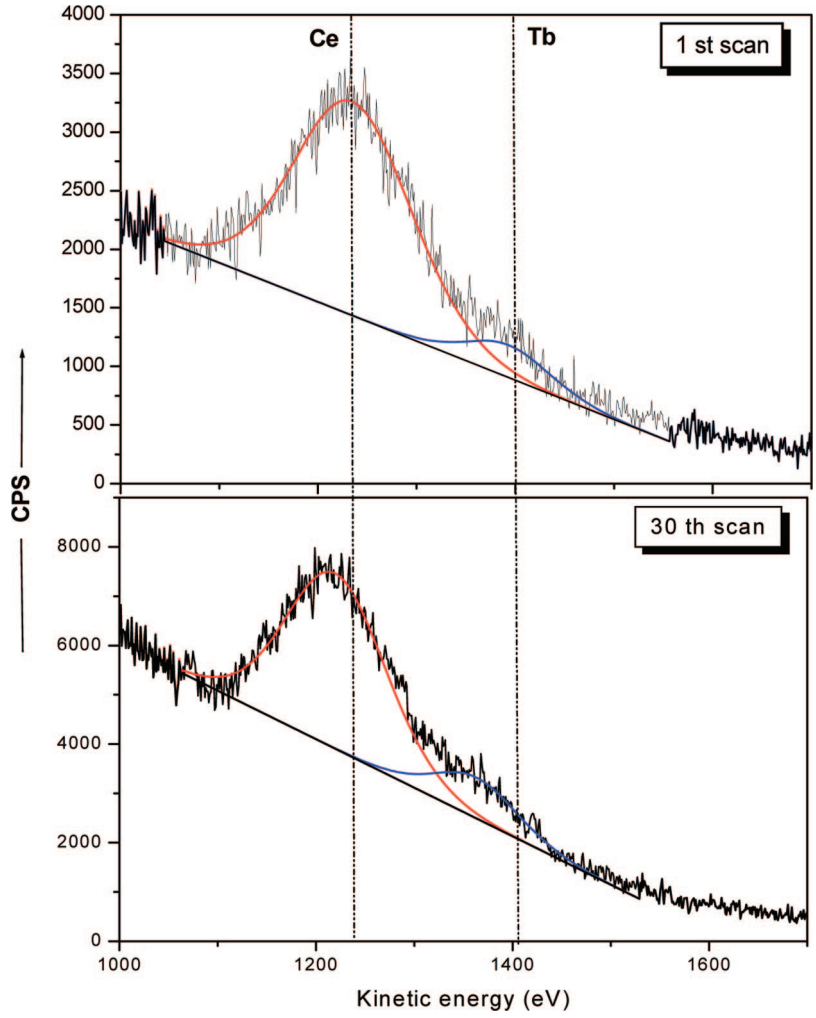

Figure 5. ISS pattern of alumina-supported ceria−terbia (CTA) sample calcined at 773 K after the 1st and 30th scans.

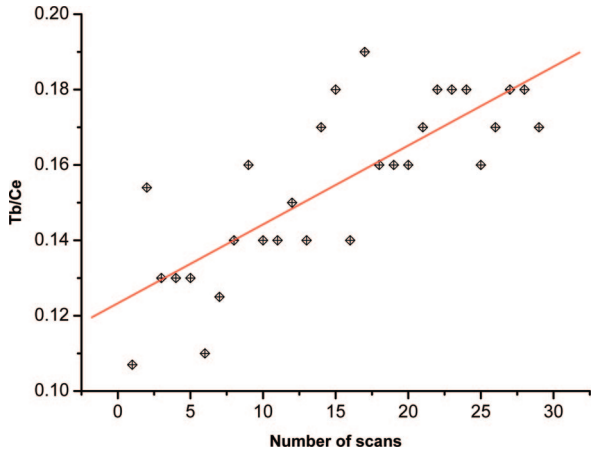

Figure 6. Plot of Tb/Ce intensity ratio obtained for alumina-supported ceria−terbia (CTA) sample calcined at 773 K after different scans.

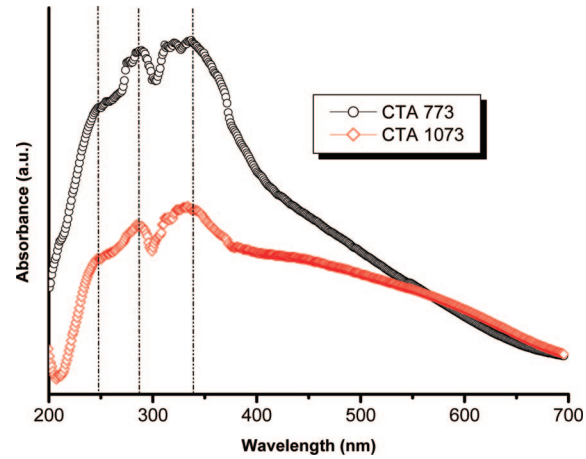

Figure 7. UV−vis DRS spectra of alumina-supported ceria−terbia (CTA) sample calcined at 773 and 1073 K.

To have insight into the surface structure at the external periphery, a series of Ar−ISS spectra were measured with the 773 K calcined sample. The first and the last (30th) scans of this series are presented in Figure 5. The main Ce peak is accompanied by a small signal ascribed to the presence of Tb. Though the two signals cannot be completely resolved, it is seen that Tb is exposed on the surface of the sample. The signals have been fitted by two components as shown in the figure. The Tb surface concentration is, however, not accessible as sensitivity factors are not available. A small shift in the position of the Ce and Tb peaks after the sputter series is observed, which is probably an instrumental problem (instability of the kinetic energy scale) encountered in heavy-ion ISS with the spectrometer used. Figure 6 shows the development of the intensity ratios between Tb and Ce, which indicate that there is a significant increase in the Tb/Ce intensity ratio during the sputter series. This means Ce is enriched at the external surface of the mixed oxide. This slight surface enrichment of Ce in the CTA sample may facilitate easy reducibility of the sample leading to better

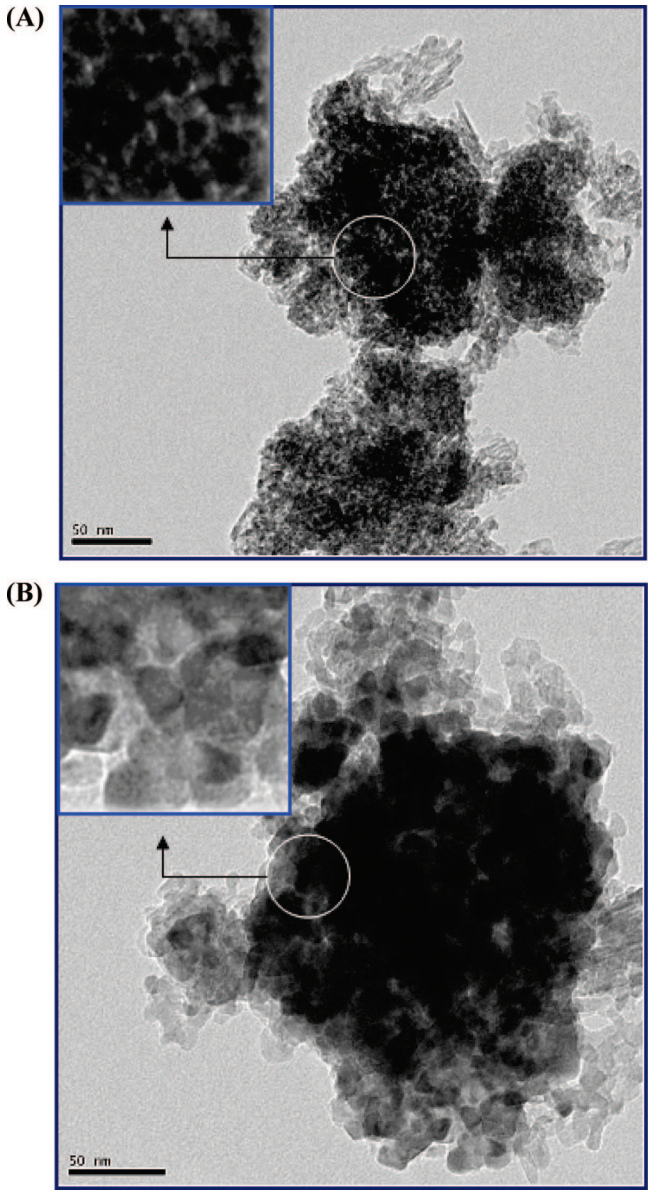

Figure 8. TEM micrographs of (A) 773 and (B) 1073 K calcined alumina-supported ceria−terbia (CTA) samples (inset: enlarged views of the encircled areas).

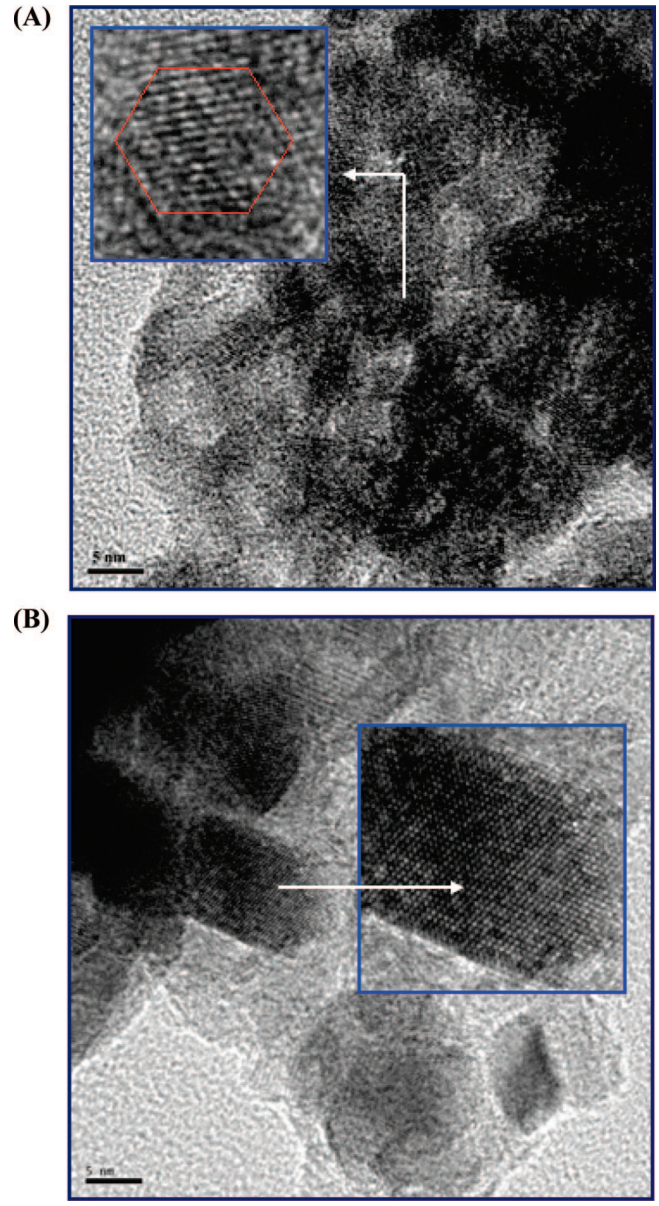

Figure 9. HREM micrographs of (A) 773 and (B) 1073 K calcined alumina supported ceria−terbia (CTA) samples (inset: enlarged views of the selected areas).

catalytic activity. Focus will be given on this aspect in the later part of our discussion.

UV−vis DRS spectra of CTA samples calcined at 773 and 1073 K and recorded in the 200−700 nm range are shown in Figure 7. It is known that pure CeO_2 exhibits three absorption maxima centered at ~255, 285, and 340 nm in its DR spectra.[62] The latter two absorption maxima are ascribed to $Ce^{4+} \leftarrow O^{2-}$ charge transfer and interband transitions, respectively.[63] The former maxima corresponds to $Ce^{3+} \leftarrow O^{2-}$ charge transfer transitions.[64] Specular reflectance effects produced by the strong absorption of ceria in the UV range may lead to such nature of the patterns. Though it might affect the shape of the interband transition, the absorption edge position has not been modified remarkably. In the present case, the absorption edge is blue-shifted (~246, 286, and 332 nm) with respect to ceria. This blue shift may be the result of decreasing particle size of ceria (quantum size effect) when terbium is incorporated into the ceria lattice as evidenced by XRD analysis.[63,64] Also, it may be due to an increasing contribution of $Ce^{4+} \leftarrow O^{2-}$ charge transfer, which is more prominent in the case of small crystallites (localized effect).[35] It is interesting to note that the band at ~246 nm, which has been characterized as $Ce^{3+} \leftarrow O^{2-}$ charge transfer transition, is also well resolved in the case of both samples investigated. This implies the occurrence of oxygen vacancy defects in the samples corroborating with the Raman spectroscopy studies. There is no clue for the presence of other phases like terbia in agreement with XRD and Raman measurements.

To uncover the information on the nanometer sizes of the investigated oxide samples, TEM−HREM analysis was performed and some representative micrographs are included. The TEM and HREM micrographs pertaining to 773 and 1073 K calcined samples are presented in Figures 8A,B and 9 A,B, respectively. The insets in the figures correspond to the enlarged views of some selected portions. In all the images, small, well-faceted mixed oxide particles deposited on the surface of larger support crystals are clearly visible. The mixed oxide crystals seem to be well distributed on the support, i.e., homogeneous in nature. It is a known fact that control of microstructures is an important factor for the improvement of OSC and catalytic

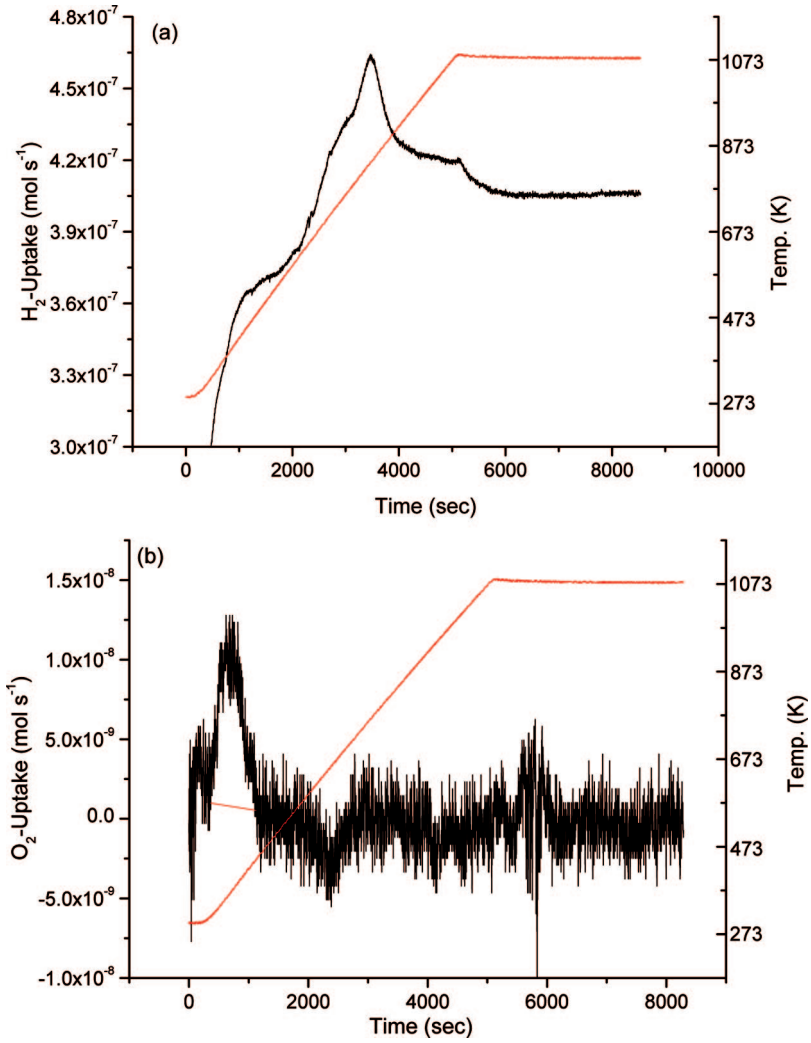

Figure 10. TPR−TPO patterns of 773 K calcined alumina-supported ceria−terbia (CTA) sample: (a) first TPR run and (b) first TPO run.

activity in such systems.[47] HREM micrographs provide a better perception of the size and dispersion of these mixed oxide particles. As observed, the mixed oxide particles are agglomerated in nature. Plain faces representing the support could not be seen suggesting the amorphous nature of it. This observation is backed by the XRD results as well. The shapes of the particles are more or less cuboctahedral. Digital diffraction patterns (DDP) for some selected particles revealed lattice spacings at 0.31 and 0.27 nm characteristic of the fluorite type structure with [110] orientation.[31] Some overlapping regions of the mixed oxide particles are seen in the HREM images, which may be responsible for better catalytic activity. As can be seen from Figures 8A and 9A, the 773 K calcined sample exhibits mixed oxide particle dimensions of ∼4−5 nm. A small increase in particle size (up to ∼8−10 nm) with temperature increase to 1073 K is revealed by Figures 8B and 9B.

The reduction/oxidation properties of the CTA sample calcined at 773 K was investigated with the TPR−TPO method and the results are shown in Figures 10 and 11. As can be noticed from Figure 10a, the first TPR profile is composed of two overlapping peaks. The reduction of the sample starts at around 380 K having its maximum at 473 K. The reduction in this low-temperature region can be attributed to the reduction of surface ceria.[45] Before the first peak could be resolved completely, the second peak appeared (centered at ∼773 K), which could be ascribed to the reduction of bulk ceria.[45] For pure ceria, due to low surface area, the low-temperature reduction feature generally appears as a very weak signal.[45] The broad nature of the low-temperature TPR peak revealing high H_2 consumption in the present case (Figure 10a) may be due to significant increase in the surface area. No characteristic peaks could be found for Tb^{4+} to Tb^{3+} transformation, which is generally observed at the temperature range of ∼576, 940, and 993 K. It is well-known that the addition of terbia to ceria results in the lowering of the reduction temperature of ceria that is caused by partial substitution of Ce^{4+} by Tb^{4+}. We have found that the reduction of Ce−Tb oxide occurs in the range of 473−873 K, whereas that of pure ceria occurs beyond 873 K.[11] After incorporation of alumina support, the reduction temperature has been lowered further (∼380−773 K). This is an interesting observation from this investigation. Alumina-supported ceria−terbia sample is therefore expected to show better catalytic activity. In the first TPO profile (Figure 10b) of the reduced sample, the reoxidation peak is observed starting at ∼323 K and centered at ∼355 K. At this temperature range the sample may not become completely reoxidized as a noisy small hype is observed at ∼773 K. The second TPR profile (Figure 11a) shows that the sample is capable of being highly reduced after the first TPR−TPO cycle. Here too, the profile consists of overlapping peaks and it is difficult to resolve those peaks. However, it can be observed that the reduction starts at ∼473 K and the most prominent reduction peak is centered at below 873 K. The reduction temperatures are thus increased in comparison to the first TPR run, which can be rationalized due

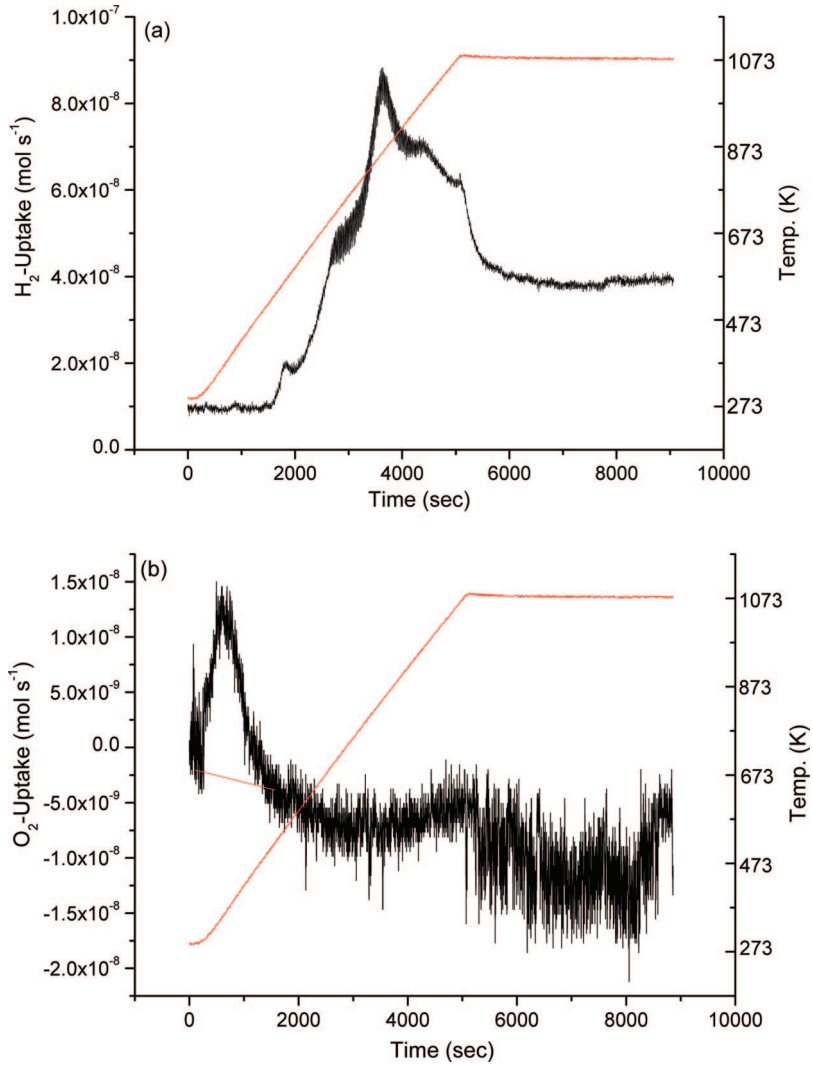

Figure 11. TPR−TPO patterns of 773 K calcined alumina-supported ceria−terbia (CTA) sample: (a) second TPR run and (b) second TPO run.

to an increase in particle size and decrease of surface area after treating the sample up to 1073 K. The similarity of the first and the second TPR profiles suggests that the mixed oxide did not change much after the first TPR−TPO cycle. However, if we compare the H_2 consumption values of the first TPR and second TPR profiles (obtained by integrating the signals recorded), we could see that the value of the second TPR run is lower than that of the first one. So, there is a possibility that after the first TPR run, some interaction between the mixed oxide and the support might occur. However, XRD and XPS analyses did not provide any evidence regarding the formation of $LnAlO_3$ (Ln = Ce or Tb). At this situation, therefore, it is not possible to draw any concrete conclusion. We cannot rule out the possibility of formation of amorphous aluminate that may be crystallized at higher temperatures beyond 1073 K. Like the first TPO profile, the second TPO profile (Figure 11b) also reveals one main reoxidation peak centered at ~373 K. Another small hype is observed at ~900 K. The most important point to note here is that the sample after severe heat treatment is also capable of showing prominent redox activity. Therefore, the catalyst is highly thermostable and the structure and morphology of the catalyst has not changed irreversibly.

The OSC property of ceria has been known as a primary criterion to catalyze oxidation reactions, particularly CO oxidation. The reaction of oxygen release from pure ceria can be written as:

$$CeO_2 \rightarrow Ce_2O_3 + {}^1/_2O_2 \quad (1)$$

During this transformation, oxygen vacancies are created in the ceria lattice. Indeed the value of vacancy content/concentration (δ) is very small and therefore the more accurate reaction for this transformation with small structural changes in ceria lattice can be described as:

$$Ce^{4+}{}_{1-x}Tb_xO_2 \rightarrow (Ce^{4+}{}_{1-2\delta}Ce^{3+}{}_{2\delta})_{1-x}Tb_xO_{2-\delta} + \delta/2O_2 \quad (2)$$

In the present case, we obtained a δ value of 0.36 (562 μmol of O_2/g of CT) for the CTA sample corresponding to 1.14% weight loss in the second cycle of the heat treatment in the thermogravimetric method. For unsupported CT sample, we obtained a δ value of 0.18 (170 μmol of O_2/g of CT) corresponding to 0.55% weight loss.[11] This is indeed a positive observation as these values are quite high in comparison to some previous reports related to ceria-based mixed oxides.[47] However,

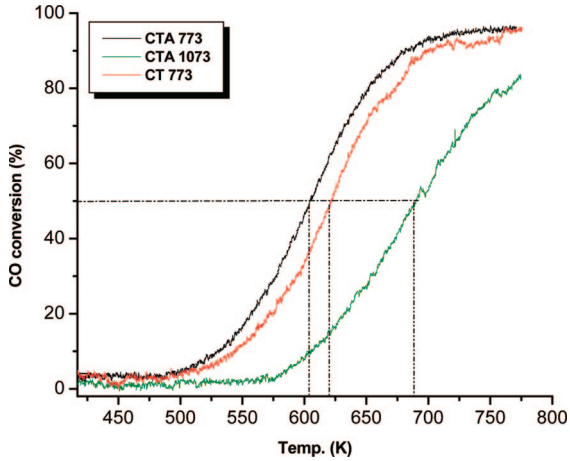

Figure 12. Conversion of CO over alumina-supported ceria−terbia (CTA) samples calcined at 773 and 1073 K, and unsupported ceria−terbia (CT) sample calcined at 773 K as a function of reaction temperature.

it must be kept in mind that the method of OSC calculation is very sensitive to the experimental conditions and the values may change drastically with change in conditions of experiment. But, it is clear that the OSC of the ceria−terbia mixed oxide is enhanced when alumina support is employed. This may be due to the increased dispersion of the mixed oxide over the support with significant increase in the surface area. Also, XRD analysis revealed the fluorite-type structure of the CTA sample, which is known to be an important parameter for better OSC.

The catalytic activity for CO oxidation of CTA samples calcined at 773 and 1073 K in the temperature range of 400 to 773 K is represented in Figure 12. For comparison purposes, the CO oxidation activity result obtained for unsupported ceria−terbia (CT, 773 K calcined) sample is also included in the figure. It is evident from the figure that all the samples exhibited very good activity in terms of total conversion and light off temperatures (temperature at 50% conversion). The CTA sample calcined at 773 K exhibited ∼100% conversion at 730 K with a light off temperature at 604 K whereas 773 K calcined unsupported ceria−terbia sample exhibited ∼100% CO conversion at ∼773 K with a light off temperature at 622 K.[11] This shows the superiority of the CTA sample over unsupported CT sample. The 1073 K calcined CTA sample also exhibited ∼85% conversion at 773 K. There is a small difference of light off temperatures for CTA samples calcined at 773 and 1073 K. This might be due to the following effects: (1) the loss of surface area, increase in particle size, and formation of more agglomerated microstructures losing dispersion of the active mixed metal oxide; (2) phase transformation of the mixed oxide; and (3) a change in the redox state in the mixed oxide. From our previous discussion, it is clear that neither phase transformation nor remarkable change in the redox state of the mixed oxides occur up to the temperature of 1073 K. Hence, loss of dispersion might affect the activity. As discussed in the TPR−TPO analysis, however, we must consider the effect of change in the redox state also, because some portion of the Ce−Tb mixed oxide might interact with the alumina support to form amorphous aluminate (s), leading to some changes in the redox states of the Ce and/or Tb. However, from the obtained results it is obvious that the CTA sample has the promising characteristics to be used as a catalyst in the modern TWC catalyst formulations.

Conclusions

(i) Ceria−terbia mixed oxides dispersed over Al_2O_3 support possessing high specific surface area and good thermal stability were successfully synthesized by a deposition coprecipitation method. (ii) The X-ray diffraction analysis revealed the crystal faces corresponding to a fluorite-type structure of ceria−terbia solid solution and there is no indication of formation of other compounds such as $LnAlO_3$ (Ln = Ce, Tb). (iii) Raman spectroscopy studies revealed the formation of oxygen vacancies in the mixed oxide lattice. (iv) The XPS analysis suggested the presence of both Ce and Tb in 3+ and 4+ oxidation states. There was no formation of any mixed oxide phase between alumina and ceria and/or terbia as supported by XRD analysis. (v) ISS analysis suggested surface enrichment of cerium, which is evident from the Tb/Ce intensity ratio in the sputter series. (vi) The UV−vis DRS measurements indicated the lowering of symmetry and consequent strain development at the cerium sites. (vii) The TEM−HREM studies showed that the particles of supported ceria−terbia solid solutions have the dimension of ∼3.7−11.5 nm within the investigated temperature range. (viii) The OSC and CO oxidation activity of the resulting sample was found to be substantially high due to the formation of solid solution and higher defect sites in its crystal lattice, higher dispersion of the active phase over the support, and easy reducibility.

Acknowledgment. The authors are thankful to Dr. Tetsuo Umegaki, AIST-Kansai, Japan, and Dr. Sergij Merzlikin and Ms. S. Buse, RUB, Germany for help in XPS, ISS, and TPR−TPO measurements, respectively. P.S. and P.B. thank the Council of Scientific and Industrial Research (CSIR), New Delhi for senior research fellowships. Thanks are due to DST, New Delhi and DAAD, Germany for financial support under a bilateral collaboration program (DST-DAAD-PPP-2005).

References and Notes

(1) Trovarelli, A. In *Catalysis by Ceria and Related Materials*, Catalytic Science Series; Hutchings, G. J., Ed.; Imperial College Press: London, UK, 2002; Vol. 2.
(2) Kaspar, J.; Fornasiero, P.; Graziani, M. *Catal. Today* **1999**, *50*, 285.
(3) Di Monte, R.; Kaspar, J. *J. Mater. Chem.* **2005**, *15*, 633.
(4) Di Monte, R.; Fornasiero, P.; Desinan, S.; Kaspar, J.; Gatica, J. M.; Calvino, J. J.; Fonda, E. *Chem. Mater.* **2004**, *16*, 4273.
(5) Reddy, B. M.; Bharali, P.; Saikia, P.; Park, S.-E.; van den Berg, M. W. E.; Muhler, M.; Grünert, W. *J. Phys. Chem. C* **2008**, *112*, 11729.
(6) Wang, J.; Wen, J.; Shen, M. *J. Phys. Chem. C* **2008**, *112*, 5113.
(7) Schwartz, J. M.; Schmidt, L. D. *J. Catal.* **1994**, *148*, 22.
(8) Korsvik, C.; Patil, S.; Seal, S.; Self, W. T. *Chem. Commun.* **2007**, 1056.
(9) Zhou, G.; Gorte, R. J. *J. Phys. Chem. B* **2008**, *112*, 9869.
(10) Zafiris, G. S.; Gorte, R. J. *J. Catal.* **1993**, *139*, 561.
(11) Reddy, B. M.; Saikia, P.; Bharali, P.; Yamada, Y.; Kobayashi, T.; Muhler, M.; Grünert, W. *J. Phys. Chem. C* **2008**, *112*, 16393.
(12) Wang, S.; Lu, G. Q. *Appl. Catal. B* **1998**, *19*, 267.
(13) Montoya, J. A.; Romero-Pascual, E.; Gimon, C.; Del Angel, P.; Monzon, A. *Catal. Today* **2000**, *63*, 71.
(14) Liao, L.; Mai, H. X.; Yuan, Q.; Lu, H. B.; Li, J. C.; Liu, C.; Yan, C. H.; Shen, Z. X.; Yu, T. *J. Phys. Chem. C* **2008**, *112*, 9061.
(15) Masui, T.; Fujiwara, K.; Machida, K. I.; Adachi, G. Y. *Chem. Mater.* **1997**, *9*, 2197.
(16) Bernal, S.; Blanco, G.; Cifredo, G. A.; Delgado, J. J.; Finol, D.; Gatica, J. M.; Izquierdo, J. M. R.; Vidal, H.; Hoser, A. *Chem. Mater.* **2002**, *14*, 844.
(17) Balducci, G.; Islam, M. S.; Kaspar, J.; Fornasiero, P.; Graziani, M. *Chem. Mater.* **2000**, *12*, 677.
(18) Fernandez-Garcia, M.; Martinez-Arias, A.; Iglesias-Juez, A.; Belver, C.; Hungria, A. B.; Conesa, J. C.; Soria, J. *J. Catal.* **2000**, *194*, 385.
(19) Ozaki, T.; Masui, T.; Machida, K.; Adachi, G.; Sakata, T.; Mori, H. *Chem. Mater.* **2000**, *12*, 643.
(20) Vidal, H.; Kasper, J.; Pijolat, M.; Colon, G.; Bernal, S.; Cordon, A.; Perrichon, V.; Fally, F. *Appl. Catal. B* **2001**, *30*, 75.
(21) Lopez, A.-B.; Krishna, K.; Makkee, M.; Moulijn, J. A. *J. Catal.* **2005**, *230*, 237.
(22) Reddy, B. M.; Bharali, P.; Saikia, P.; Khan, A.; Loridant, S.; Muhler, M.; Grünert, W. *J. Phys. Chem. C* **2007**, *111*, 1878.

(23) Vidmar, P.; Fornasiero, P.; Kaspar, J.; Graziani, M. *J. Catal.* **1997**, *171*, 160.
(24) Ohashi, T.; Yamazaki, S.; Tokunaga, T.; Arita, Y.; Matsui, T.; Harami, T.; Kobayashi, K. *Solid State Ionics* **1998**, *113*−*115*, 559.
(25) Pu, Z. Y.; Lu, J. Q.; Luo, M. F.; Xie, Y. L. *J. Phys. Chem. C* **2007**, *111*, 18695.
(26) Hungria, A. B.; Martinez-Arias, A.; Fernandez-Garcia, M.; Iglesias-Juez, A.; Ruiz, A. G.; Calvino, J. J.; Conesa, J. C.; Soria, J. *Chem. Mater.* **2003**, *15*, 4309.
(27) Bernal, S.; Blanco, G.; Cauqui, M. A.; Corchado, P.; Pintado, J. M.; Izquierdo, J. M. R. *Chem. Commun.* **1997**, 1545.
(28) Vries, K. J. D.; Meng, G. Y. *Mater. Res. Bull.* **1998**, *33*, 357.
(29) Wang, X.; Hanson, J. C.; Liu, G.; Rodriguez, J. A. *J. Chem. Phys.* **2004**, *121*, 5434.
(30) Martinez-Arias, A.; Hungria, A. B.; Fernandez-Garcia, M.; Iglesias-Juez, A.; Conesa, J. C.; Mather, G. C.; Munuera, G. *J. Power Sources* **2005**, *151*, 43.
(31) Galtayries, A.; Blanco, G.; Cifredo, G. A.; Finol, D.; Pintado, J. M.; Vidal, H.; Sporken, R.; Bernal, S. *Surf. Interface Anal.* **1999**, *27*, 941.
(32) Zamar, F.; Trovarelli, A.; de Leitenburg, C.; Dolcetti, G. *Stud. Surf. Sci. Catal.* **1996**, *101*, 1283.
(33) Bernal, S.; Blanco, G.; Cauqui, M. A.; Corchado, M. P.; Larese, C.; Pintado, J. M.; Izquierdo, J. M. R. *Catal. Today* **1999**, *53*, 607.
(34) Martinez-Arias, A.; Hungria, A. B.; Fernandez-Garcia, M.; Conesa, J. C.; Munuera, G. *J. Power Sources* **2005**, *151*, 32.
(35) Martinez-Arias, A.; Fernandez-Garcia, M.; Salamanca, L. N.; Valenzuela, R. X.; Conesa, J. C.; Soria, J. *J. Phys. Chem. B* **2000**, *104*, 4038.
(36) Aboussaid, K.; Bernal, S.; Blanco, G.; Cifredo, G. A.; Galtayries, A.; Pintado, J. M.; el Begrani, M. S. *Surf. Interface Anal.* **2008**, *40*, 250.
(37) Bigey, C.; Hilaire, L.; Maire, G. *J. Catal.* **2001**, *198*, 208.
(38) Pantu, P.; Kim, K.; Gavalas, G. R. *Appl. Catal. A* **2000**, *193*, 203.
(39) Trovarelli, A. *Catal. Rev. Sci. Eng.* **1996**, *38*, 439.
(40) Damyanova, S.; Perez, C. A.; Schmal, M.; Bueno, J. M. C. *Appl. Catal. A* **2002**, *234*, 271.
(41) Miki, T.; Ueno, A.; Matsura, S.; Sato, M. *Chem. Lett.* **1998**, 565.
(42) Shyu, J. Z.; Weber, W. H.; Gandhi, H. S. *J. Phys. Chem.* **1988**, *94*, 6464.
(43) Graham, G. W.; Schmitz, P. J.; Usmen, R. K.; McCabe, R. W. *Catal. Lett.* **1993**, *17*, 175.
(44) Piras, A.; Trovarelli, A.; Dolcetti, G. *Appl. Catal. B* **2000**, *28*, L77.
(45) Piras, A.; Colussi, S.; Trovarelli, A.; Sergo, V.; Liorca, J.; Psaro, R.; Sordelli, L. *J. Phys. Chem. B* **2005**, *109*, 11110.
(46) Bernal, S.; Calvino, J. J.; Cifredo, G. A.; Finol, D.; Gatica, J. M.; Kiely, C. J.; Cartes, C. L.; Zheng, J. G.; Vidal, H. *Chem. Mater.* **2002**, *14*, 1405.
(47) Ozawa, M.; Matuda, K.; Suzuki, S. *J. Alloys Compd.* **2000**, *303*−*304*, 56.
(48) Klug, H. P.; Alexander, L. E. In *X-ray diffraction Procedures for Polycrystalline and Amorphous Materials*, 2nd ed.; John Wiley and Sons: New York, 1974.
(49) Wagner, C. D.; Riggs, W. M.; Davis, L. E.; Moulder, J. F. In *Handbook of X-ray Photoelectron Spectroscopy*; Muilenberg, G. E., Ed.; Perkin-Elmer Corporation: Eden Prairie, MN, 1978.
(50) Logan, A. D.; Shelef, M. *J. Mater. Res.* **1994**, *9*, 468.
(51) Reddy, B. M.; Khan, A. *Catal. Surv. Asia* **2005**, *9*, 155.
(52) Reddy, B. M.; Rao, K. N.; Reddy, G. K.; Khan, A.; Park, S.-E. *J. Phys. Chem. C* **2007**, *111*, 18751.
(53) Wachs, I. E. *Catal. Today* **1996**, *27*, 437.
(54) Chua, Y. T.; Stair, P. C.; Wachs, I. E. *J. Phys. Chem. B* **2001**, *105*, 8600.
(55) Dutta, P. K.; Zaykoski, R. E. *Zeolites* **1988**, *8*, 179.
(56) Reddy, B. M.; Lakshmanan, P.; Bharali, P.; Saikia, P.; Thrimurthulu, G.; Muhler, M.; Grünert, W. *J. Phys. Chem. C* **2007**, *111*, 10478.
(57) Jehng, J.-M. *J. Phys. Chem. B* **1998**, *102*, 5816.
(58) Normand, F. L.; Fallah, J. E.; Hilaire, L.; Legare, P.; Kotani, A.; Parlebas, J. C. *Solid State Commun.* **1989**, *71*, 885.
(59) Li, L.; Wei, Q.; Li, H.; Zhang, D.; Su, W. *Z. Phys. B* **1995**, *96*, 451.
(60) Blanco, G.; Pintado, J. M.; Bernal, S.; Cauqui, M. A.; Corchado, M. P.; Galtayries, A.; Ghijsen, J.; Sporken, R.; Eickhoff, T.; Drube, W. *Surf. Interface Anal.* **2002**, *34*, 120.
(61) Dufresne, P.; Payen, E.; Grimblot, J.; Bonnelle, J. P. *J. Phys. Chem.* **1981**, *85*, 2344.
(62) Reddy, B. M.; Bharali, P.; Thrimurthulu, G.; Saikia, P.; Katta, L.; Park, S.-E. *Catal. Lett.* **2008**, *123*, 327.
(63) Bensalem, A.; Muller, J. C.; Verduraz, F. B. *J. Chem. Soc., Faraday Trans.* **1992**, *88*, 153.
(64) Bensalem, A.; Verduraz, F. B.; Delamar, M.; Bugli, G. *Appl. Catal.* **1995**, *121*, 81.

JP809837G